Applied Catalysis B: Environmental 163 (2015) 179–188

Contents lists available at ScienceDirect

Applied Catalysis B: Environmental

journal homepage: www.elsevier.com/locate/apcatb

High-efficiency photoelectrochemical electrodes based on $ZnIn_2S_4$ sensitized ZnO nanotube arrays

Jianhua Han, Zhifeng Liu*, Keying Guo, Bo Wang, Xueqi Zhang, Tiantian Hong

School of Materials Science and Engineering, Tianjin Chengjian University, 300384 Tianjin, China

ARTICLE INFO

Article history:
Received 12 May 2014
Received in revised form 15 July 2014
Accepted 21 July 2014
Available online 27 July 2014

Keywords:
ZnO
$ZnIn_2S_4$
Nanotubes
Photoelectrochemical
Water splitting

ABSTRACT

Well aligned ZnO nanorods (NRs) and nanotubes (NTs) based core/shell nanoarrays were fabricated by hydrothermal chemical conversion and directional chemical etching method and used as photoelectrochemical (PEC) electrodes. The experimental results reveal that the optimum structure is the ZnO/ZnS/$ZnIn_2S_4$ NT arrays, such a novel PEC electrode has attained a hydrogen generation efficiency of 8.86%. This better result is attributed to the enhanced absorption efficiency, appropriate gradient energy gap structure and fast electron transfer rate of one-dimensional (1D) NT, which implies a promising application in PEC water splitting. In this paper, we also focus our study on the correlation between the properties of PEC electrode and the nanoarrays structure (including nanorods and nanotubes, binary and ternary sensitizer, buffer layer), and the formation mechanism of NT based on chemical etching process. By adjusting the amount of reactants and reaction time, the core/shell nanostructure can be tuned from NR to NT and formed buffer layer.

1. Introduction

Photoelectrochemical (PEC) splitting of water into hydrogen and oxygen by means of semiconductor nanomaterials has been considered as an ideal solution for environment and energy crisis [1–3], because it can convert the solar energy to storable chemical energy directly (such as hydrogen energy) [4,5]. Since Fujishima and Honda demonstrated to produce the hydrogen using PEC water splitting in 1972 [6], numerous active semiconductor materials (such as TiO_2 [7] and ZnO [8] etc.) have been proven to be able to serve as the photoelectrodes of PEC system [9,10]. In spite of TiO_2 is the most commonly studied in photoelectrode of PEC system, ZnO has been considered as an ideal replacement to TiO_2 owing to its similar energy band structure and higher photogenerated electron transfer rate [11,12]. What is more, ZnO can be simply synthesized to various morphology, such as nanotube, nanowire and nanotree etc. [13–15]. Among the variety of nanostructures, one-dimensional (1D) ZnO nanostructure (such as nanotube and nanowire etc.) can provide a direct electrical pathway without crystal boundary resistance [12,16,17]. Therefore, it is important to adopt 1D ZnO NT arrays as photoelectrode of PEC system due to its high specific surface area and photoelectrons transport properties [18,19]. So far, various methods for synthesizing core/shell tubular ZnO-based nanoarrays have been employed, such as electrochemical method [20], wet chemical method [21], hydrothermal method [22] and template-based growth [23]. Nevertheless, it is a grand challenge to synthesis large-scale growth of ZnO-based NT arrays with uniform morphology and structure. A novel technique to overcome these disadvantages for large-scale fabrication of well-aligned ZnO-based NT arrays is to apply a simple process based on directional chemical etching.

However, bare ZnO photoelectrode can respond only to ultraviolet (UV) region due to its wide band gap, which just accounts for 4% of the sunlight [24,25]. In order to extend the absorption spectrum to the visible light region, numerous efforts have been done (such as elemental doping and sensitizing with the quantum dots) [26–29]. Sensitizing with the quantum dots (QDs) has been identified as an effective route for PEC system due to the outstanding photoelectrical properties of QDs sensitizers and its similarities with dye-sensitized photoelectrode [30–32]. Among the various QDs sensitizers, CdS, PbS etc. demonstrate high photocatalytic activity in PEC system, but their toxicity threats our health and environment seriously. Ternary Zinc indium sulfide ($ZnIn_2S_4$), which has a suitable band gap (2.34–2.48 eV) according with the visible light region and ideal chemical stability for PEC water splitting, has attracted considerable attention [33,34]. For $ZnIn_2S_4$ sensitized ZnO PEC electrode, $ZnIn_2S_4$ offers favorable energetic for photoelectric since its conduction band edge is more negative than ZnO [35,36]. To our

* Corresponding author. Tel.: +86 22 23085236; fax: +86 22 23085110.
E-mail address: tjulzf@163.com (Z. Liu).

http://dx.doi.org/10.1016/j.apcatb.2014.07.040
0926-3373/

best knowledge, although $ZnIn_2S_4$ has showed high photocatalytic activity, there are few reports about the PEC electrode of $ZnIn_2S_4$ served as sensitizer in water splitting. Moreover, it is known that, in a core/shell nanostructure, the introduction of a buffer layer between core and shell can enhance the device performance owing to (a) the buffer layer optimizes the band configuration of the structure; (b) it increases excess carrier lifetime; (c) it improves lattice matching at the heterojunction interface [37,38]. Lee et al. reported a synthetic route to a $CuInS_2$/CdS/ZnO NR structure for a thin film solar cell with a buffer of CdS [38].

Motivated by the above concerns, herein, we firstly fabricated the $ZnIn_2S_4$ sensitized 1D ZnO nanoarrays with a buffer layer of ZnS via a simple chemical conversion method and a convenience directional chemical etching process. Compared with the traditional methods, the chemical route is easy to be controlled and obtained uniform structure, which can decrease defects of the products [8]. In the present study, the effects of reaction time and solution concentration on the core/shell structure and PEC activity of photoelectorde were investigated. Meanwhile, the formation mechanism of NT by chemical etching process was discussed in detail according to the experimental results. Finally, ZnO NT arrays with a buffer of ZnS and sensitized by $ZnIn_2S_4$ QDs were fabricated to apply in PEC system, the calculated efficiency for hydrogen production of the samples was evaluated to be up to 8.86%. It is founded that the excellent performance is attributed to the enhanced absorption efficiency and appropriate gradient energy gap structure. These results provide new insight in the development of ternary sensitizer QDs sensitized ZnO-based photoelectode for PEC water splitting.

2. Experimental

2.1. Preparation of ZnO nanorod arrays

The ZnO NR arrays were directly grown on the indium tin oxide (ITO) glass substrates [39]. In a typical synthesis process, firstly, the ITO substrates were ultrasonically rinsed for 0.5 h in acetone, isopropyl alcohol and ethanol absolution, respectively. The seed layer was deposited on ITO via a sol–gel and dip-coating method. Then the substrates with seed layer were annealed at 400 °C for 60 min, followed by the incubation in the aqueous solution containing 0.05 M zinc nitrate and 0.05 M hexamethylenetetramine at 90 °C for 4 h. The prepared samples of ZnO NR films were washed with deionized water and dried in air.

2.2. Synthesis of ZnO/ZnS nanorod (nanotube) arrays

The ZnO/ZnS NR arrays were prepared via a chemical conversion process by immersing the ZnO NR arrays in aqueous solutions containing 0.02 M thiacetamide (TAA) at 90 °C for 7 h. Meanwhile, the ZnO/ZnS NT films of different reaction time were synthesized via a directional chemical etching by immersing the ZnO NR arrays in aqueous solutions containing 0.1 M TAA at 90 °C for 1 h, 5 h and 7 h, respectively. The as-obtained samples were washed with deionized water and dried in air.

2.3. Fabrication of $ZnIn_2S_4$ sensitized ZnO nanoarrays

In a Teflon-lined stainless steel autoclave, samples of ZnO/ZnS NR and NT arrays were immersed in triethylene glycol (TEG) containing 5 mM $InCl_3$, respectively. The samples of ZnO/ZnS/$ZnIn_2S_4$ NR and ZnO/ZnS/$ZnIn_2S_4$ NT arrays were prepared when the autoclave was sealed and maintained at 200 °C for 3 h. After being naturally cooled to room temperature, the products were washed with absolute ethanol and dried in air. Meanwhile, samples of ZnO/ZnS NT arrays were immersed in TEG containing 10 mM $InCl_3$, and the auto-clave was sealed and maintained at 200 °C for 5 h, then the ZnO/$ZnIn_2S_4$ NT arrays were obtained. The as-prepared products were washed with absolute alcohol and dried in air.

2.4. Characterization

Morphology and structure of the samples were characterized using HITACHI S-4800I field emission scanning electron microscope (FE-SEM) and JEOL JEM-2100F transmission electron microscopy (TEM) operated at an accelerating voltage of 100 kV. The EDS mapping of the samples analysis were also performed during the FE-SEM observation. The X-ray diffraction (XRD) patterns of samples were performed using a Rigaku D/max-2500 using Cu Kα radiation (λ = 0.154059 nm). DU-8B UV/VIS double-beam spectrophotometer was used to achieve the optical absorption spectra of the photoelectrode. PEC properties characterization of the products were determined using an electrochemical workstation (LK2005A, Tianjin, China), a three-electrode configuration, with ZnO-based nanoarrays on ITO as the working photoelectrode, 1 M Na_2S solution as electrolyte, saturated Ag/AgCl as reference electrode, and a platinum (Pt) foil as counter electrode. Meanwhile, photocurrents of the samples were measured under the irradiation of a xenon lamp (100 mW cm^{-2}) with global AM 1.5 G. The hydrogen generation efficiencies (η) of the photoelectrodes were calculated by the following equation [40]:

$$\eta = \left[\frac{I(1.23 - E_{bias})}{J_{light}}\right] \times 100\% \quad (1)$$

where I is the photocurrent density (mA cm^{-2}), 1.23 the theoretical potential required for water splitting, E_{bias} the applied external potential and J_{light} the intensity of the simulated incident solar light, which is 100 mW cm^{-2} in this study. To estimate the correlation between light absorption and photocurrent density on diverse PEC electrodes, incident photon-to-current-conversion efficiency (IPCE) measurements were performed under a constant potential of 0.2 V versus Ag/AgCl. IPCE values were calculated using the following equation [41]:

$$\text{IPCE} = \left[\frac{1240 J_p}{\lambda I_{light}}\right] \times 100\% \quad (2)$$

where J_p is the photocurrent density (mA cm^{-2}), I_{light} is the incident light irradiance (100 mW cm^{-2}), and λ is the incident light wavelength (nm).

3. Results and discussion

In this work, 1D $ZnIn_2S_4$ sensitized ZnO nanoarrays (including NT and NR) were successfully fabricated through a facile hydrothermal chemical method. The effect of preparation parameters on the structure of the product was studied by adjusting the pH value of solution, the concentration of the TAA solution (or $InCl_3$ solution) and the reaction time. The synthetic route of $ZnIn_2S_4$ sensitized 1D ZnO nanoarrays is schematically illustrated in Fig. 1. The hexagonal ZnO NR arrays were initially prepared on ITO substrates via a hydrothermal method (Step 1). In this step, the ZnO seed layer was fabricated after sintering and developed into ZnO NRs in the growth solution. It is well known that chemical conversion process based on the ion-by-ion growth mechanism would take place spontaneously when there are sufficient differences in the solubility products constants (K_{sp}) between the reactants and the products. When the ITO substrate coated with ZnO NR arrays is immersed into 0.02 M TAA solution, the sulfidation of ZnO will take place producing TAA hydrolyzes and H_2S gas (the chemical reactions happened are as Eq. (3)) [42–44], it is because of the large difference between

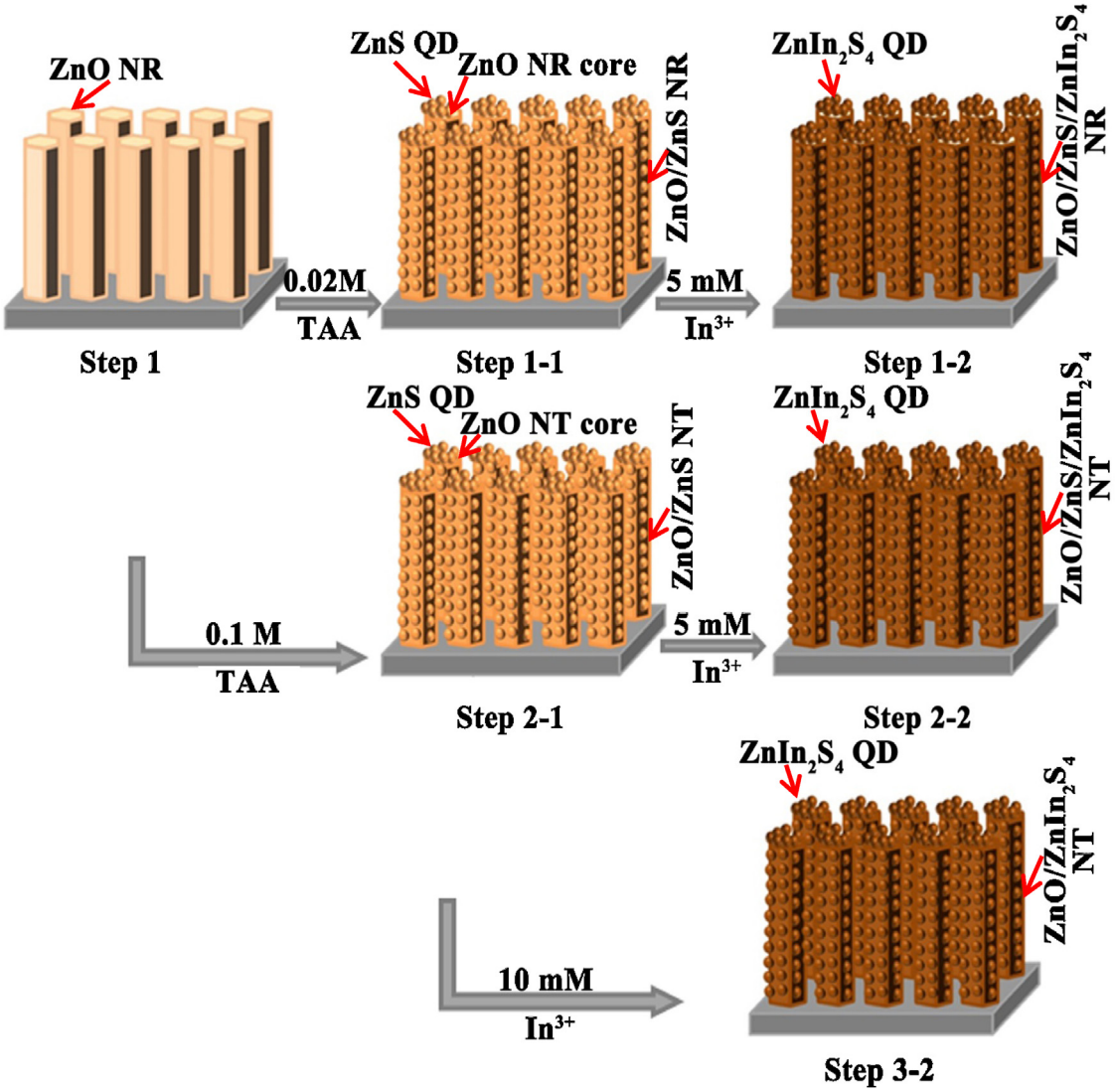

Fig. 1. Schematic illustration for the synthesis $ZnIn_2S_4$ sensitized 1D ZnO nanoarrays.

the solubility product constants (K_{sp}) of ZnO (6.8×10^{-17}) and ZnS (2.93×10^{-25}).

$$CH_3CSNH_2 + H_2O \rightarrow CH_3CONH_2 + H_2S \quad (3)$$

The further reaction of ZnO with H_2S around the surface of the NRs leads to the formation of ZnO/ZnS core/shell NRs (Step 1-1) (Fig. 2(a)). Nevertheless, when the sample is immersed into 0.1 M TAA solution, the ZnO NRs will convert to ZnO/ZnS NTs (Step 2-1) (Fig. 2(d)), and the synthetic route of ZnO/ZnS NT arrays was showed in Fig. 2(e), which is attributed to the TAA solution in high concentration can produce more hydrogen ion, and thus the pH was reduced significantly. As an amphoteric oxide, ZnO NRs can react with H^+ in TAA solution and the products are soluble salts (Eq. (5)), with the increase of H^+ concentration, the chemical etching process on ZnO NRs was gradually enhanced. According to our experimental results, ZnO/ZnS NRs are formed by chemical etching on the outside surface of NRs in 0.02 M TAA solution (Fig. 2(a)), ZnO/ZnS NTs are formed by selective etching on the (0 0 1) polar planes of NRs in 0.1 M TAA solution (Fig. 2(d)). The chemical reactions and the thermodynamic deduction of reactions happened are as following [45]:

$$\Delta G = G_{(product)} - G_{(reactant)} \quad (4)$$

$$\Delta G = \Delta H - T\,\Delta S \quad (5)$$

$$H_2S \rightarrow 2H^+ + S^{2-} \quad (6)$$

$\Delta G = 119.36\ kJ\ mol^{-1}$; $\Delta H = 53.73\ kJ\ mol^{-1}$; $\Delta S = -220.39\ J\ mol^{-1}$; $T = 298\ K$;

$$ZnO + S^{2-} + H_2O \rightarrow ZnS + 2OH^- \quad (7)$$

$\Delta G = -46.15\ kJ\ mol^{-1}$;

$$ZnO + 2H^+ \rightarrow Zn^{2+} + H_2O \quad (8)$$

$\Delta G = -65.89\ kJ\ mol^{-1}$;

It is known that the chemical reactions occur spontaneously when $\Delta G < 0$, which means that the chemical reaction of Eqs. (7) and (8) will occurred. It can be seen that the ΔG of Eq. (6) was higher than zero, however, the temperature of chemical reactions occur spontaneously is 298 K. In our experiment, the temperature of solution is 363 K, therefore, the reactions listed above can proceed naturally. It can be concluded that the concentration of TAA solution plays an important role in the formation of ZnO/ZnS nanoarrays during the hydrothermal chemical progress. And the structure (NR or NT) can be controlled by altering the concentration of the TAA solution.

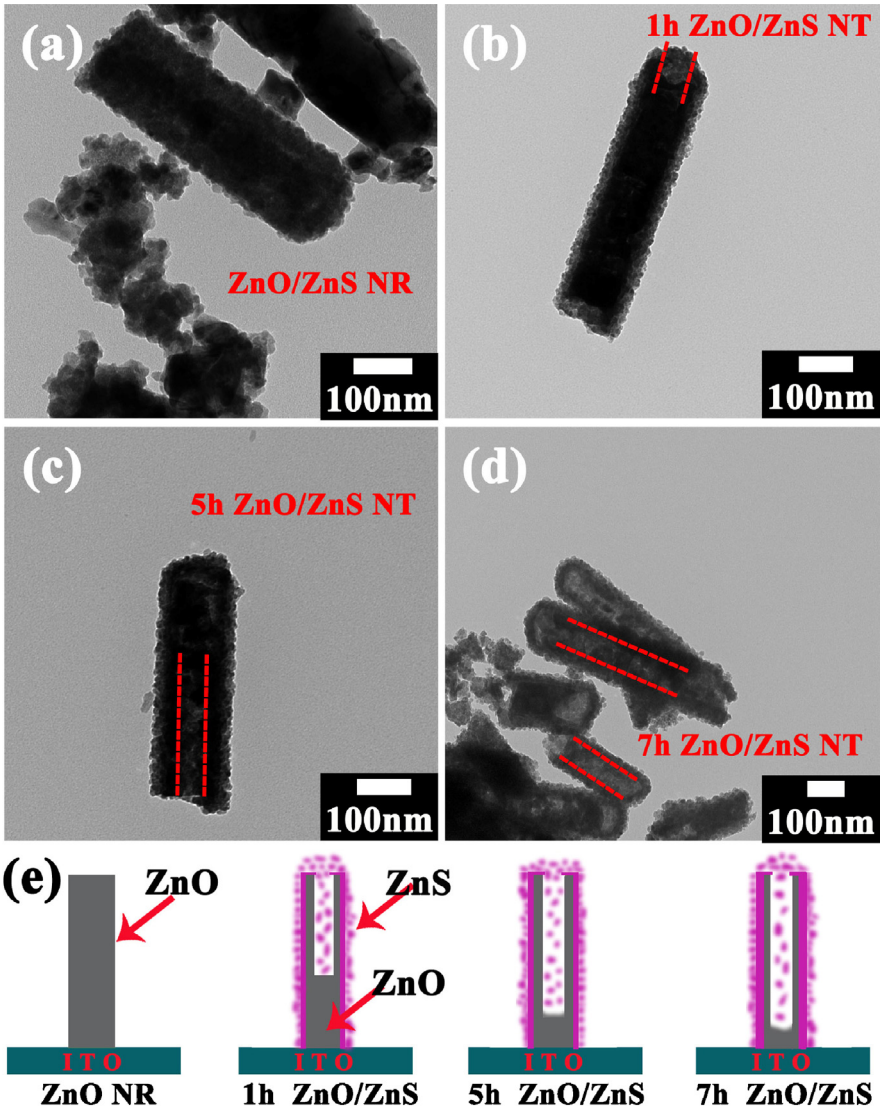

Fig. 2. TEM images of [ZnO/ZnS NR (a)] (0.02 M TAA) and [1 h ZnO/ZnS NT (b), 5 h ZnO/ZnS NT (c), 7 h ZnO/ZnS NT (d)] (0.1 M TAA); Schematic illustration for the synthesis of ZnO/ZnS NT arrays (e).

The preparation of ternary chalcogenides ($ZnIn_2S_4$) is operated in an auto-clave. Finally, $ZnIn_2S_4$ shell was obtained after ZnS reacting with enough In^{3+} in the triethylene glycol (TEG) solvent. When the ITO substrate with ZnO/ZnS NRs (NTs) was immersed in 5 mM $InCl_3$ solution for 3 h, ZnS shell was partially converted to $ZnIn_2S_4$. In this step, the ZnO/ZnS/$ZnIn_2S_4$ NRs (NTs) could be obtained by using ZnO/ZnS NRs (NTs) as reactive templates, a buffer layer of ZnS and a ternary sensitizer layer of $ZnIn_2S_4$ were formed at the same time.

In order to investigate the forming process of ZnO/ZnS NTs, ZnO NRs were etched in different concentrations of solution and at different reaction time. Fig. 2(a) shows the TEM image of ZnO NRs in 0.02 M TAA solution for 7 h, Fig. 2(b–d) shows the TEM images of ZnO NRs in 0.1 M TAA solution at different periods. Fig. 2(a) presents a typical TEM image of ZnO/ZnS NR obtained by immersing the ZnO NRs in 0.02 M TAA solution for 7 h, the result reveals that the ZnO NR is fully covered with a ZnS shell, the diameter of NRs is about 130 nm. As displayed in Fig. 2(b), a slender hollow structure was formed in the center part of the product after being etched in TAA solution for 1 h. When the etching time increased to 5 h (Fig. 2(c)), the hollow structure is bigger, the diameter of hollow structure is about 50 nm. When etching time was reached to 7 h (Fig. 2(d)), ZnO/ZnS NTs with thin-wall were obtained. In brief, the diameter of hollow structure increased gradually with increasing etching time. It can be seen clearly from the above experimental results (Fig. 2(a–d)), the ZnO/ZnS NRs (NTs) with arbitrary thickness can be synthesized by adjusting the etching time in TAA solution (adjusting the concentration of TAA solution). The ZnO/ZnS nanotubes could be obtained in the low pH when the concentration of TAA solution is 0.1 M. On the contrary, the ZnO/ZnS nanorods could be formed under low concentration of TAA solution (0.2 M).

On the basis of the TEM images of ZnO NRs in TAA solution at different periods, the formation route of the ZnO/ZnS NT arrays can be proposed as a directional chemical etching mechanism, which is illustrated in Fig. 2(e). In this chemical etching process, the ZnO NRs can be transformed into ZnO/ZnS NTs after treatment in acidic solutions. In aqueous TAA solution, ZnO NRs can react with H^+ in acid solution and the products are soluble salts. Therefore, the chemical etching process will occur when the ZnO NRs were immersed in TAA solution. It is generally known that the etching process is directional and mainly focused on the center of NRs, which is attributed to the metastability of the (0 0 1) plane with high surface energy [13]. As a result, the etching rate of (0 0 1) polar plane is faster than that of nonpolar plane, the directional etching of ZnO along

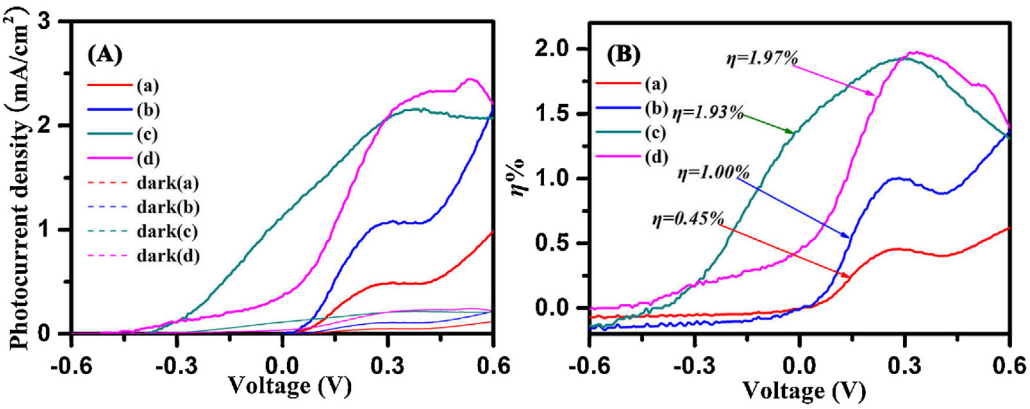

Fig. 3. Photocurrent density–voltage curves under the irradiation of AM 1.5 G and dark condition (A) and photoconversion efficiency (B) of as-prepared 1 h ZnO/ZnS NT (a), 5 h ZnO/ZnS NT (b), ZnO/ZnS NR (c) and 7 h ZnO/ZnS NT (d).

the *c*-axis causes the formation of the NT arrays. With the etching time increasing, the depth of the NT gradually increased. In this work, chemical etching process starts from the top surface of NR, and then the chemical etching process mainly focused on the inner of NR. Eventually, the NTs were covered up because of many ZnS nanoparticles accumulated on the pipe orifice.

To further analyze the correlation between the properties of PEC electrode and the NRs (NT) structure, PEC performance of ZnO-based nanoarrays photoelectrodes was performed using an electrochemical workstation. Fig. 3(A) shows the photocurrent density–voltage curves under the irradiation of AM 1.5 G and dark condition of as-prepared 1 h ZnO/ZnS NTs, 5 h ZnO/ZnS NTs, ZnO/ZnS NRs and 7 h ZnO/ZnS NTs, respectively. It can be seen that the current of samples under dark condition was very low, therefore, the majority of measured current is photocurrent. Furthermore, Table 1 displays the photocurrent density and efficiencies of hydrogen generation of as-obtained samples. It can be seen that the photocurrent densities of 1 h ZnO/ZnS NT, 5 h ZnO/ZnS NT, ZnO/ZnS NR and 7 h ZnO/ZnS NT were 0.47 mA cm^{-2} at 0.278 V versus Ag/AgCl, 1.06 mA cm^{-2} at

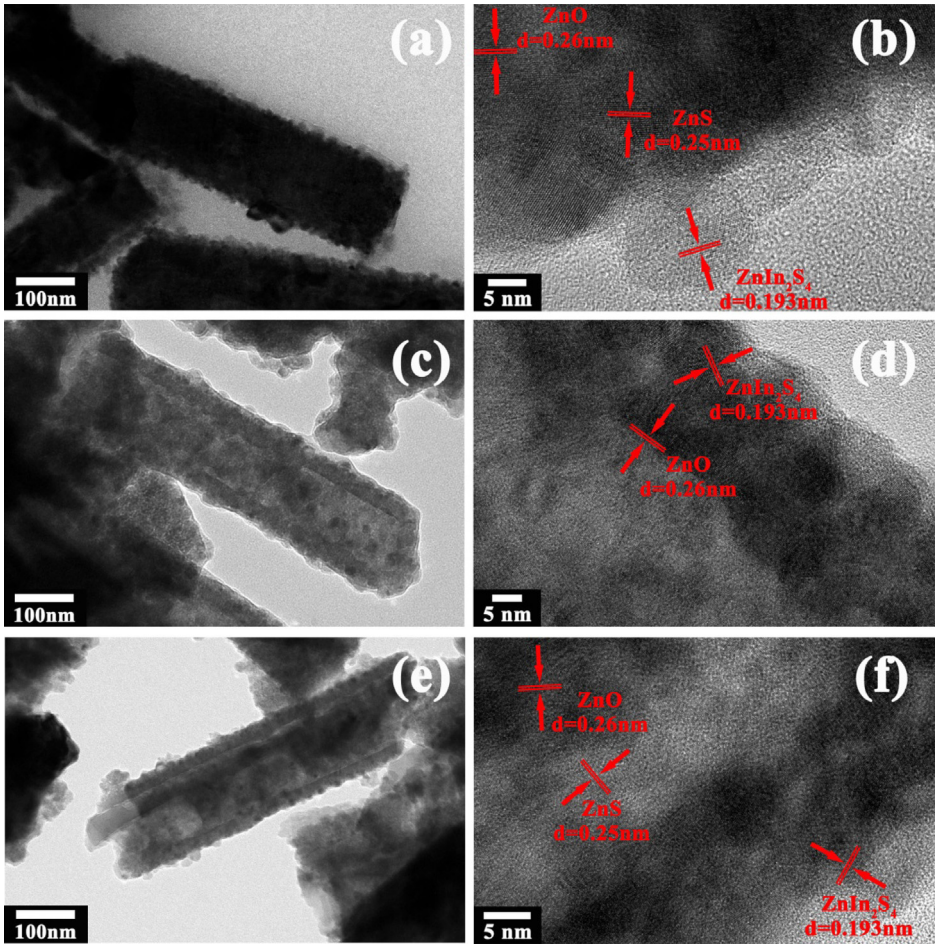

Fig. 4. TEM images of ZnO/ZnS/$ZnIn_2S_4$ NR (a), ZnO/$ZnIn_2S_4$ NT (c) and ZnO/ZnS/$ZnIn_2S_4$ NR (e); HRTEM images of ZnO/ZnS/$ZnIn_2S_4$ NR (b), ZnO/$ZnIn_2S_4$ NT (d) and ZnO/ZnS/$ZnIn_2S_4$ NR (f).

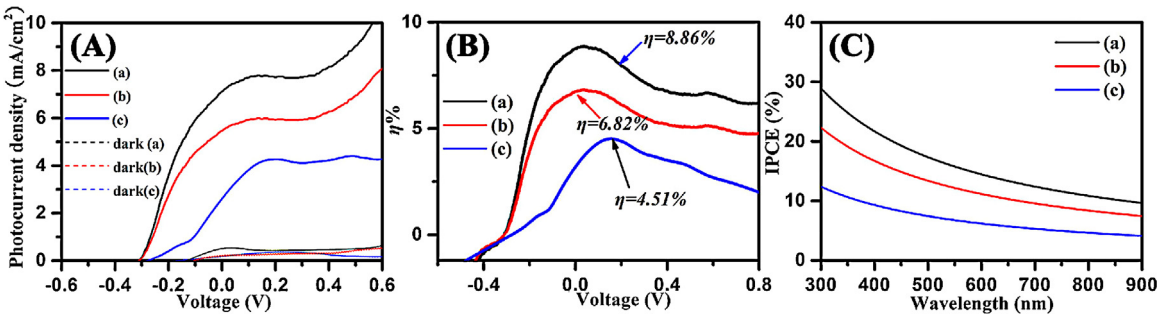

Fig. 5. Photocurrent density–voltage curves under the irradiation of AM 1.5 G and dark condition (A), photoconversion efficiency (B) and IPCE plots in the range of 300–900 nm (C) of as-prepared ZnO/ZnS/$ZnIn_2S_4$ NT (a), ZnO/ZnS/$ZnIn_2S_4$ NR (b) and ZnO/$ZnIn_2S_4$ NT (c).

0.288 V versus Ag/AgCl, 2.10 mA cm^{-2} at 0.312 V versus Ag/AgCl, 2.21 mA cm^{-2} at 0.338 V versus Ag/AgCl, respectively, measured in Na_2S electrolyte (1 mol/L) under irradiation with simulated light of AM 1.5 G. Accordingly, as shown in Fig. 3(C), the theoretical efficiencies of hydrogen generation of as-prepared 1 h ZnO/ZnS NT, 5 h ZnO/ZnS NT, ZnO/ZnS NR and 7 h ZnO/ZnS NT were 0.45%, 1.00%, 1.93% and 1.97%, respectively. The maximum efficiency of hydrogen production of 1.97% was calculated, indicating that the shell thickness was a key factor for PEC performance.

To understand the interrelation between reaction parameters and nanostructure (such as buffer layer, hollow structure), various samples (ZnO/ZnS/$ZnIn_2S_4$ NR, ZnO/$ZnIn_2S_4$ NT and ZnO/ZnS/$ZnIn_2S_4$ NT) were synthesized by adjusting the concentration of $InCl_3$ and the reaction time. Furthermore, these structures were characterized using transmission electron microscopy (TEM) and high resolution transmission electron microscopy (HRTEM). Fig. 4(a and b) shows the TEM images and the HRTEM images of ZnO/ZnS/$ZnIn_2S_4$ NR, respectively. It can be seen that the sample is a trilaminar core/shell NR with a diameter of about 130 nm, the surface of NR appears to be relatively smooth, and some nanoparticles are accumulated on the surface. As shown in Fig. 4(b), the HRTEM image clearly presents three distinct sets of lattice fringes, where the crystal lattice fringes spacing are 0.26 nm, 0.25 nm and 0.193 nm, corresponding to the ZnO, ZnS and $ZnIn_2S_4$, respectively. Fig. 4(c and d) shows the TEM and HRTEM images of ZnO/$ZnIn_2S_4$ NT, respectively, where the bistratal core/shell nanostructure can be clearly observed. The diameter of NT is about 130 nm, and the $ZnIn_2S_4$ nanoparticles are uniformly covered around the NT surface. From the HRTEM image in Fig. 4(d), two distinct sets of lattice fringes are corresponding to the ZnO and $ZnIn_2S_4$, respectively. Fig. 4(e and f) shows the TEM and HRTEM images of ZnO/ZnS/$ZnIn_2S_4$ NT, respectively. The sample is a trilaminar NT with a diameter of about 130 nm, and the buffer layer of ZnS can be clearly observed. The HRTEM investigation (Fig. 4(f)) reveals the trilaminar NT is composed of ZnO, ZnS and $ZnIn_2S_4$. From the above observations and analyses of TEM and HRTEM, as we expected, bistratal and trilaminar $ZnIn_2S_4$ sensitized ZnO core/shell nanoarrays (NR and NT) were synthesized successfully.

Table 1
The photocurrent density and efficiencies of hydrogen generation of samples.

Photoelectrode	E_{bias}	I (mA cm^{-2})	η (%)
ZnO NR	0.212	0.41	0.42
1 h ZnO/ZnS NT	0.278	0.47	0.45
5 h ZnO/ZnS NT	0.288	1.06	1.00
ZnO/ZnS NR	0.312	2.10	1.93
7 h ZnO/ZnS NT	0.338	2.21	1.97
ZnO/ZnS/$ZnIn_2S_4$ NR	0.038	5.72	6.82
ZnO/$ZnIn_2S_4$ NT	0.156	4.20	4.51
ZnO/ZnS/$ZnIn_2S_4$ NT	0.039	7.44	8.86

In order to further investigate the correlation between the PEC performance of electrode and the nanostructure (such as buffer layer, hollow structure) more explicitly, $ZnIn_2S_4$ sensitized ZnO nanoarrays photoelectrodes were fabricated to determine the PEC properties. Fig. 5(A) shows the photocurrent density–voltage curves under the irradiation of AM 1.5 G and dark condition of as-obtained ZnO/ZnS/$ZnIn_2S_4$ NT, ZnO/ZnS/$ZnIn_2S_4$ NR and ZnO/$ZnIn_2S_4$ NT, respectively. The current of samples in dark condition was very low, so we can concluded that the majority of measured current is photocurrent. What is more, the photocurrent density and hydrogen generation efficiencies of products were presented in Table 1. The photocurrent densities of ZnO/ZnS/$ZnIn_2S_4$ NR, ZnO/$ZnIn_2S_4$ NT and ZnO/ZnS/$ZnIn_2S_4$ NT were 5.72 mA cm^{-2} at 0.038 V versus Ag/AgCl, 4.20 mA cm^{-2} at 0.156 V versus Ag/AgCl, 7.44 mA cm^{-2} at 0.039 V versus Ag/AgCl, respectively. Correspondingly, as shown in Fig. 5(B), the theoretical efficiencies of hydrogen generation of as-prepared ZnO/ZnS/$ZnIn_2S_4$ NR, ZnO/$ZnIn_2S_4$ NT and ZnO/ZnS/$ZnIn_2S_4$ NT were 6.82%, 4.51% and 8.86%, respectively. Fig. 5(C) presents the IPCE plots of ZnO/ZnS/$ZnIn_2S_4$ NR, ZnO/$ZnIn_2S_4$ NT and ZnO/ZnS/$ZnIn_2S_4$ NT, it can be seen that the ZnO/ZnS/$ZnIn_2S_4$ NT photoelectrode exhibited highest photoactivity in visible light. Besides, IPCE profile of ZnO/ZnS/$ZnIn_2S_4$ NT PEC electrodes is found broadened and strengthened over the entire wavelength region compared with that of ZnO/ZnS/$ZnIn_2S_4$ NR, ZnO/$ZnIn_2S_4$ NT PEC electrodes.

Based on the above analyses, ZnO/ZnS/$ZnIn_2S_4$ NT PEC electrode showed the highest hydrogen generation efficiency, revealing that ZnS buffer layer and hollow NT structure were more suitable for absorb photons and separate electrons and holes. It is well known that buffering techniques can inhibit the formation of interface traps and defect states, prolong the excess carrier lifetime. In such an energy gap configuration (Fig. 6), a buffer layer of ZnS between ZnO and $ZnIn_2S_4$ can enhance the device performance

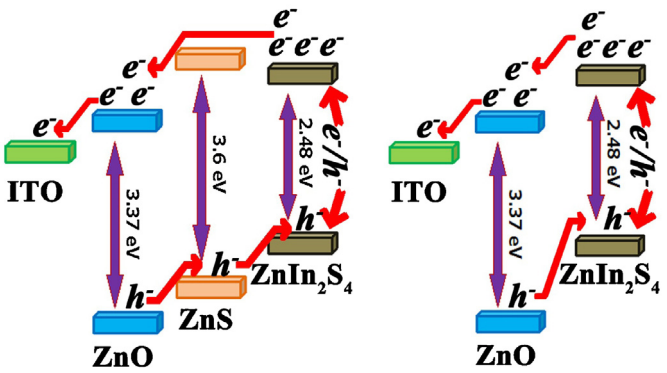

Fig. 6. Schematic diagram illustrating the energy levels of ITO/ZnO/ZnS/$ZnIn_2S_4$ and ITO/ZnO/$ZnIn_2S_4$ heterostructure.

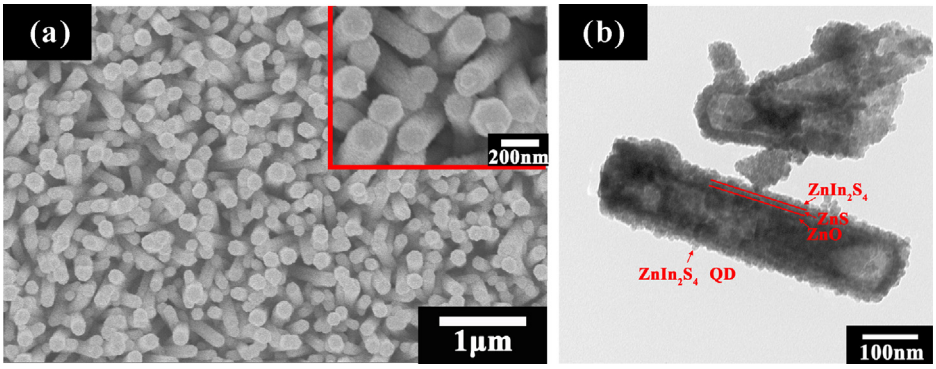

Fig. 7. SEM images and enlarged view SEM images (a), TEM images (b) of ZnO/ZnS/$ZnIn_2S_4$ NT arrays.

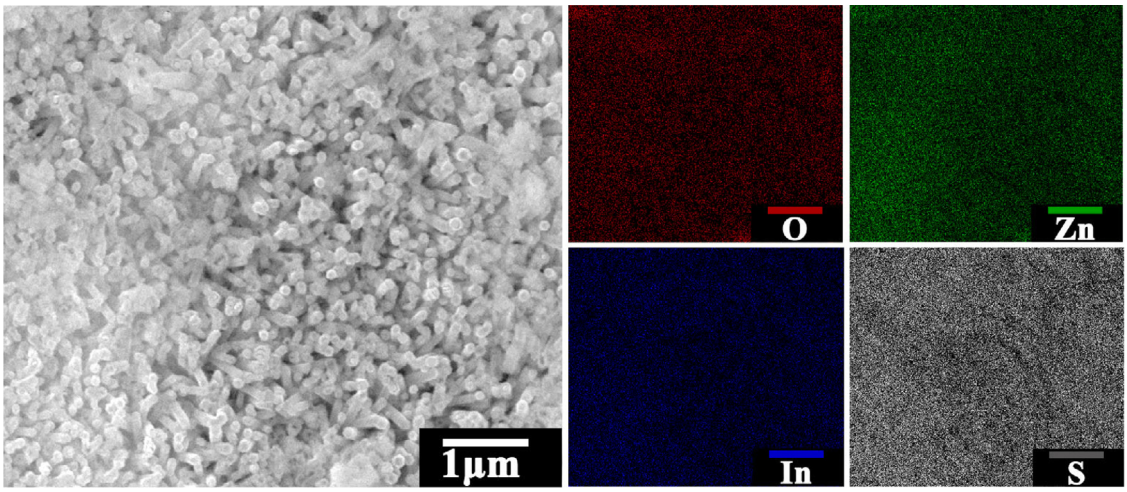

Fig. 8. Elemental distribution mapping of ZnO/ZnS/$ZnIn_2S_4$ NT arrays.

by avoiding undesirable shunt path and widening the depletion width that extend electricfield in absorber layer and minimize the collection loss by tunneling and recombination. As a consequence, the gradient energy gap structure can improved the separation and transmission of photogenerated electrons and holes significantly.

The morphology and structure of the as-prepared sample were characterized using field emission scanning electron microscope (SEM) and transmission electron microscope (TEM). Fig. 7(a) shows a SEM image of the ZnO/ZnS/$ZnIn_2S_4$ NT arrays, and the inset shows a enlarge view of the NT arrays. It can be seen clearly that the high-density NTs grow vertically aligned on the ITO substrate, and the NT presents a hexagonal shape with diameter ranging from 120 nm to 140 nm. Analysis of SEM images presents that some nanoparticles accumulated on the top of the NTs (inset of Fig. 7(a)), and thus the NTs is covered up. As depicted in Fig. 7(b), the TEM image reveals the product is a trilaminar nanotube, in which ZnO is the hollow core, $ZnIn_2S_4$ is the shell and ZnS as buffer layer between the core and shell. The surface of NTs is smooth and a lot of $ZnIn_2S_4$ quantum dots (QDs) distribute uniformly over the NT surface. And the diameter of NT is consistent with the SEM observations.

The element composition of as-prepared ZnO/ZnS and ZnO/ZnS/$ZnIn_2S_4$ were further characterized using energy dispersive spectrometer (EDS) mapping, the EDS mapping of samples are shown in Fig. 8. EDS results of ZnO/ZnS and ZnO/ZnS/$ZnIn_2S_4$ shows that elements of Zn, O, S and In can be clearly observed. It provides credible evidence for the composition of the samples includes $ZnIn_2S_4$. The composition and crystallographic structure of the ZnO NRs, ZnO/ZnS NTs and ZnO/ZnS/$ZnIn_2S_4$ NTs were determined by X-ray diffraction, as shown in Fig. 9(a–c). In Fig. 9(a), the ZnO NR presents hexagonal structure according to the standard ZnO diffraction pattern (JCPDS, No. 36-1451). Furthermore, ZnO NR preferentially grew along the [0 0 2] direction, implying that the arrays grew on the ITO substrate vertically. Fig. 9(b) shows the XRD patterns of ZnO/ZnS NT arrays, it can be seen that new peak appeared, which is in agreement with the ZnS (JCPDS, No. 12-0688), indicating that the ZnO NR arrays have been converted to ZnO/ZnS core/shell arrays already. The composition and crystallographic structure of the as-prepared ZnO/ZnS/$ZnIn_2S_4$ NTs were determined by X-ray diffraction, as shown in Fig. 9(c), the new

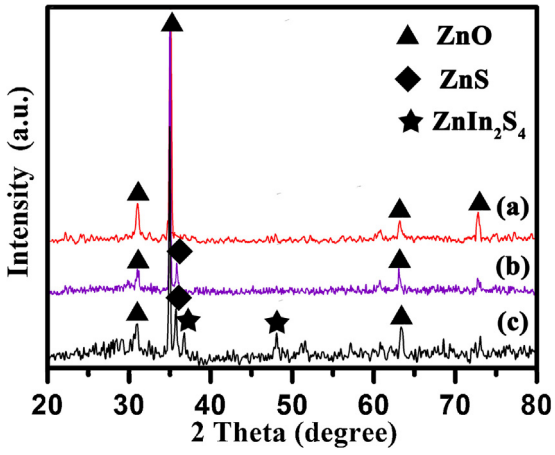

Fig. 9. XRD patterns of ZnO NRs (a), ZnO/ZnS NTs (b) and ZnO/ZnS/$ZnIn_2S_4$ NTs.

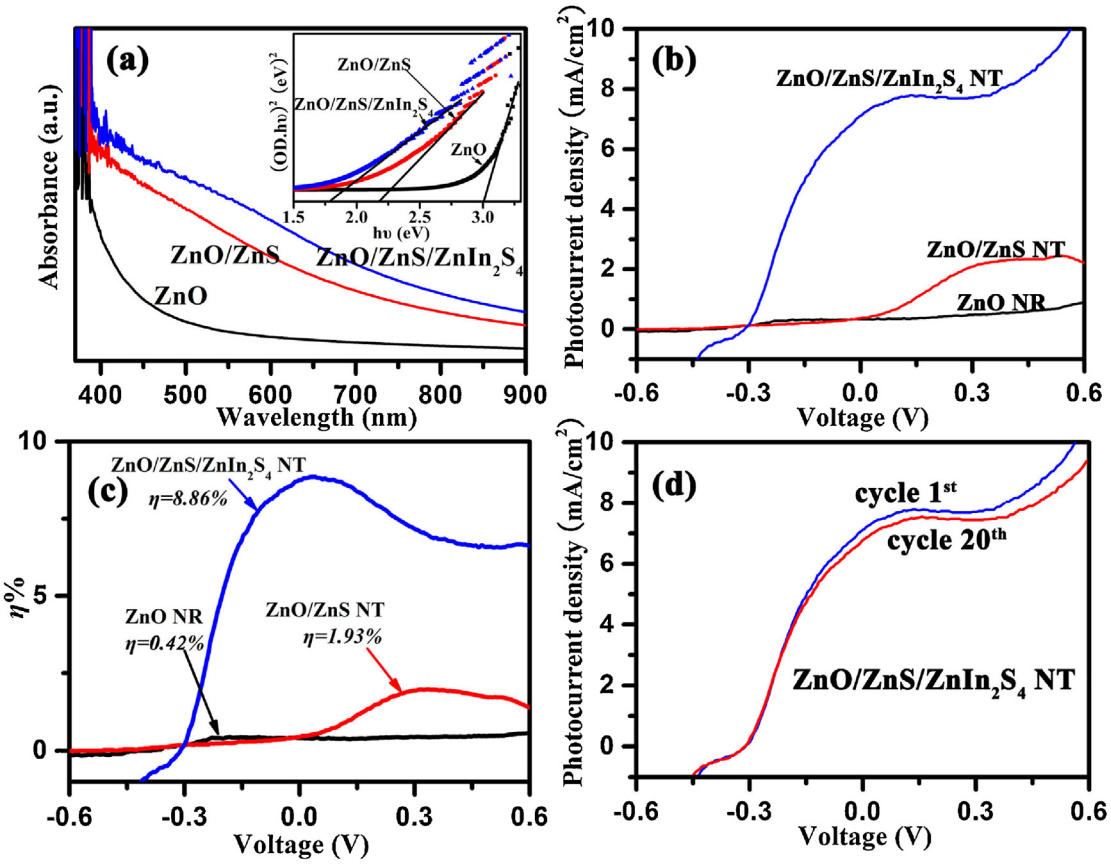

Fig. 10. UV–visible light absorption spectra (a), photocurrent density–voltage curves (b), photoconversion efficiency (c) and photocurrent density–voltage cycle times curves (d) of samples; inset of (a) shows: plot of $(OD{\cdot}h\upsilon)^2$ versus $h\upsilon$ of samples.

peaks can be well indexed to a hexagonal phase of $ZnIn_2S_4$ (JCPDS, No. 49-1562). All peaks of ZnO, ZnS and $ZnIn_2S_4$ were appeared in Fig. 9(c), which indicates that the only partial conversion of ZnS layer to $ZnIn_2S_4$, and further support that the EDS mapping results. Combined with Fig. 9(a and b), these diffraction results suggested that the ZnO/ZnS/$ZnIn_2S_4$ NT arrays can be easily prepared under the current synthetic conditions.

The optical properties of ZnO NRs, ZnO/ZnS NTs and ZnO/ZnS/$ZnIn_2S_4$ NTs were characterized by the UV–vis absorption spectra, as shown in Fig. 10(a). It can be seen that ZnO/ZnS/$ZnIn_2S_4$ NTs exhibit a remarkable red-shift compared to the ZnO NRs, and ZnO/ZnS/$ZnIn_2S_4$ NTs achieve the best efficiency of visible light absorption. Corresponding band gap of the samples are shown in inset of Fig. 10(a), the approximate band gap value of ZnO NRs, ZnO/ZnS NTs and ZnO/ZnS/$ZnIn_2S_4$ NTs are determined to be ~3.0 eV, ~2.20 eV and ~1.76 eV, demonstrating that the ZnO/ZnS/$ZnIn_2S_4$ NTs is suitable for the visible light absorption. It should be noted that the $ZnIn_2S_4$ sensitizer could improve the photo response spectrum due to the appropriate energy band gap structure (Fig. 6) and the high optical absorption coefficient of $ZnIn_2S_4$. Taking into consideration the efficient utilize of visible light in a majority of the solar spectrum, this $ZnIn_2S_4$ sensitized ZnO NT arrays based PEC electrode is an attractive semiconductor materials for water splitting. Fig. 10(b) displays the photocurrent density of ZnO NR, ZnO/ZnS NT and ZnO/ZnS/$ZnIn_2S_4$ NT, respectively. It can be seen that the photocurrent densities of ZnO NR, ZnO/ZnS NT and ZnO/ZnS/$ZnIn_2S_4$ NT were 0.41 mA cm^{-2} at 0.212 V versus Ag/AgCl, 2.21 mA cm^{-2} at 0.338 V versus Ag/AgCl, 7.44 mA cm^{-2} at 0.04 V versus Ag/AgCl, respectively, where the samples are used as photoelectrodes and Na_2S (1 mol/L) as electrolyte. Accordingly, as shown in Fig. 10(c), the theoretical efficiencies of hydrogen generation of as-prepared ZnO NR, ZnO/ZnS NT and ZnO/ZnS/$ZnIn_2S_4$ NT were 0.42%, 1.97% and 8.86%, respectively. The highest theoretical efficiency of sample showed a remarkable increment compared with the ZnO NR and the ZnO/ZnS NT. It can be concluded that the ZnO/ZnS/$ZnIn_2S_4$ NT arrays is an effective nanostructure for water splitting. Furthermore, in order to investigate the stability of as-prepared PEC electrodes, linear sweep voltammograms is measured after C-V scanning for 1 and 15 cycles under illumination, using ZnO/ZnS/$ZnIn_2S_4$ NT arrays as typical photoelectrodes. Fig. 10(d) illustrates the photocurrent density of ZnO/ZnS/$ZnIn_2S_4$ cycle 1st and ZnO/ZnS/$ZnIn_2S_4$ cycle 15th, respectively. The photocurrent densities of ZnO/ZnS/$ZnIn_2S_4$ cycle 1st and ZnO/ZnS/$ZnIn_2S_4$ cycle 15th were 7.70 mA cm^{-2} at 0.138 V and 7.56 mA cm^{-2} at 0.155 V versus Ag/AgCl, respectively. It is found obviously that the ZnO/ZnS/$ZnIn_2S_4$ arrays PEC electrode shows much more stable current density after C-V scanning under illumination for 15 cycles, revealing a better capability to resist photocorrosion.

The efficient utilization of incident sun light, the carrier injection and collection are two key factors contributing to the PEC water splitting. For the ZnO/ZnS/$ZnIn_2S_4$ NT arrays, a high efficiency of light-harvesting can be achieved by fabricating well-aligned NT arrays with high surface served as the PEC electrode, as well as, carrier injection and collection can be improved by constructing gradient energy gap configuration. The lights transfer process was shown in Fig. 11, $ZnIn_2S_4$ nanoparticles around the NT surface can reflect unabsorbed lights back to the NT arrays and the space between the nanoparticles, and thus the efficiency of light utilization is improved, which is in favor of utilization of incident

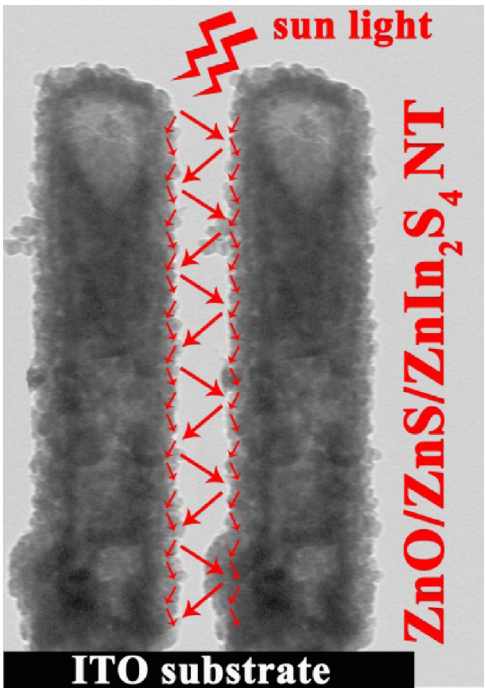

Fig. 11. Schematic representation of the utilization of incident sunlight.

sun light. Meanwhile, as a high light absorption coefficient in the visible regions materials, a layer of $ZnIn_2S_4$ can trap relatively more photons, thereby, more photons would be utilized by NT arrays for generating electron/hole pairs. Furthermore, vertical ZnO arrays on the ITO substrate can directly transport the photo-generated electrons with a high speed, which is beneficial to the carrier transport properties of the NT arrays.

The appropriate matching of the gradient energy gap structures of ZnO/ZnS/$ZnIn_2S_4$ is a key factor in the PEC water splitting process because of it can significantly increase the efficiency of carrier injection and collection. The energy gap structures of ZnO/ZnS/$ZnIn_2S_4$ and ZnO/$ZnIn_2S_4$ heterostructure are schematically illustrated in Fig. 6. As we can see from Fig. 6, both the conduction band minimum and the valance band maximum of ZnO are lower than that of $ZnIn_2S_4$. As a result, the ZnO/$ZnIn_2S_4$ composite can lead to not only transfer of electron from the conduction band of $ZnIn_2S_4$ to that of ZnO, but also transfer of hole from the valence band of ZnO to that of $ZnIn_2S_4$, and thus the efficiency of separation and transmission of electron and hole was dramatically enhanced. Based on the band gaps and the relative positions of semiconductor nanomaterials, an appropriate gradient energy gap structure was formed. It can be concluded that an excellent PEC cell was achieved by combining ZnO/$ZnIn_2S_4$ NTs with a ZnS buffer layer.

4. Conclusion

In summary, well aligned $ZnIn_2S_4$ sensitized 1D ZnO nanoarrays (NR and NT) have been fabricated on the ITO substrate via a facile and effective chemical method using ZnO nanorod as templates. Two different methods, hydrothermal chemical conversion and directional chemical etching, were used to synthesize ZnO-based core/shell nanorods arrays and ZnO-based core/shell nanotubes arrays, respectively. The formation of the ZnO/ZnS/$ZnIn_2S_4$ nanostructure (NR or NT) was associated with the solution concentration and the reaction time. By adjusting the amount of reactants and reaction time, the core/shell nanostructure can be tuned from NR to NT and formed buffer layer. The calculated efficiency of hydrogen production for ZnO/ZnS/$ZnIn_2S_4$ PEC electrode were up to 8.86%, the performance of the ZnO/ZnS/$ZnIn_2S_4$ PEC electrode was remarkably enhanced compared with the pure ZnO photoelectrode, which resulted from the broaden absorption spectrum and improved separation ability of the photogenerated electron and hole. This study demonstrates an excellent potential in the design and preparation of ZnO-based photoelectrode for PEC water splitting into hydrogen and oxygen.

Acknowledgement

The authors gratefully acknowledge the financial support from National Nature Science Foundation of China (no. 51102174).

References

[1] M. Grätzel, Nature 414 (2001) 338–344.
[2] Y.B. Li, T. Takata, D. Cha, K. Takanabe, T. Minegishi, J. Kubota, K. Domen, Advanced Materials 25 (2013) 125–131.
[3] S. Dahl, I. Chorkendorff, Nature Materials 11 (2012) 100–101.
[4] Y. Yang, K. Mielczarek, M. Aryal, A. Zakhidov, W. Hu, ACS Nano 6 (2012) 2877–2892.
[5] J.H. Bang, P.V. Kamat, ACS Nano 5 (2011) 9421–9427.
[6] A. Fujishima, K. Honda, Nature 238 (1972) 37–38.
[7] J.S. Yang, W.P. Liao, J.J. Wu, ACS Applied Materials & Interfaces 5 (2013) 7425–7431.
[8] Y.B. Li, Z.F. Liu, Y. Wang, Z.C. Liu, J.H. Han, J. Ya, International Journal of Hydrogen Energy 37 (2012) 15029–15037.
[9] Z.L. Jiang, Y.X. Tang, Q.L. Tay, Y.Y. Zhang, O.I. Malyi, D.P. Wang, J.Y. Deng, Y.K. Lai, H.F. Zhou, X.D. Chen, Z.L. Dong, Z. Chen, Advanced Energy Materials 3 (2013) 1368–1380.
[10] K. Zhang, L.J. Guo, Catalysis Science & Technology 3 (2013) 1672–1690.
[11] Z.F. Liu, Y. Wang, B. Wang, Y.B. Li, Z.C. Liu, J.H. Han, K.Y. Guo, Y.J. Li, T. Cui, L. Han, C.P. Liu, G.M. Li, International Journal of Hydrogen Energy 38 (2013) 10226–10234.
[12] J.G. Jiang, M. Wang, L.J. Ma, Q.Y. Chen, L.J. Guo, International Journal of Hydrogen Energy 38 (2013) 13077–13083.
[13] Z.F. Liu, C.C. Liu, Y. Jing, E. Lei, Renewable Energy 36 (2011) 1177–1181.
[14] D.J. Gargas, H.W. Gao, H. Wang, P.D. Yang, Nano Letters 11 (2011) 3792–3796.
[15] K.A. Dick, K. Deppert, M.W. Larsson, T. Ma¨rtensson, W. Seifert, L.R. Wallenberg, L. Samuelson, Nature Materials 3 (2004) 380–384.
[16] M. Law, L.E. Greene, J.C. Johnson, R. Saykally, P.D. Yang, Nature Materials 4 (2005) 455–459.
[17] J. Chung, J. Myoung, J. Oh, S. Lim, The Journal of Physical Chemistry C 114 (2010) 21360–21365.
[18] C.K. Xu, P. Shin, L.L. Cao, D. Gao, The Journal of Physical Chemistry C 114 (2010) 125–129.
[19] G.M. Wang, X.Y. Yang, F. Qian, J.Z. Zhang, Y. Li, Nano Letters 10 (2010) 1088–1092.
[20] Y.L. Xie, Z.X. Li, Z.G. Xu, H.L. Zhang, Electrochemistry Communications 13 (2011) 788–791.
[21] P.H. Yang, K. Wang, Z.W. Liang, W.J. Mai, C.X. Wang, W.G. Xie, P.Y. Liu, L. Zhang, X. Cai, S.Z. Tan, J.H. Song, Nanoscale 4 (2012) 5755–5760.
[22] H.B. Chen, X. Wu, L.H. Gong, C. Ye, F.Y. Qu, G.Z. Shen, Nanoscale Research Letters 5 (2010) 570–575.
[23] Y. Sun, G.M. Fuge, N.A. Fox, D.J. Riley, M.N.R. Ashfold, Advanced Materials 17 (2005) 2477–2481.
[24] M.T. Li, J.Z. Su, L.J. Guo, International Journal of Hydrogen Energy 33 (2008) 2891–2896.
[25] Y.X. Li, C.F. Xie, S.Q. Peng, G.X. Lu, S.B. Li, Journal of Molecular Catalysis A: Chemical 282 (2008) 117–123.
[26] S.H. Shen, L. Zhao, L.J. Guo, Materials Research Bulletin 44 (2009) 100–105.
[27] C.C. Liu, Z.F. Liu, J.W. Li, J.H. Han, Y. Wang, Z.C. Liu, J. Ya, Microelectronic Engineering 103 (2013) 12–16.
[28] K. Žídek, K.B. Zheng, C.S. Ponseca, M.E. Messing, L.R. Wallenberg, P. Chábera, M. Abdellah, V. Sundström, T. Pullerits, Journal of the American Chemical Society 134 (2012) 12110–12117.
[29] H.B. Wang, T. Kubo, J. Nakazaki, T. Kinoshita, H. Segawa, The Journal of Physical Chemistry Letters 4 (2013) 2455–2460.
[30] H. Kim, H. Jeong, T.K. An, C.E. Park, K. Yong, ACS Applied Materials & Interfaces 5 (2013) 268–275.
[31] P.V. Kamat, The Journal of Physical Chemistry C 112 (2008) 18737–18753.
[32] Y.L. Lee, Y.S. Lo, Advanced Functional Materials 19 (2009) 604–609.
[33] Y.G. Yu, G. Chen, G. Wang, Z.S. Lv, International Journal of Hydrogen Energy 38 (2013) 1278–1285.
[34] S.H. Shen, L. Zhao, Z.H. Zhou, L.J. Guo, The Journal of Physical Chemistry C 112 (2008) 16148–16155.
[35] H.M. Jia, W.W. He, Y. Lei, X.W. Chen, Y. Xiang, S. Zhang, W.M. Lau, Z. Zheng, RSC Advances 3 (2013) 8909–8914.
[36] K.S. Leschkies, T.J. Beatty, M.S. Kang, D.J. Norris, E.S. Aydil, ACS Nano 3 (2009) 3638–3648.
[37] M.A. Contreras, M.J. Romero, B. To, F. Hasoon, R. Noufi, S. Ward, K. Ramanathan, Thin Solid Films 403–404 (2002) 204–211.

[38] D. Lee, K. Yong, ACS Applied Materials & Interfaces 4 (2012) 6758–6765.
[39] Z.F. Liu, L.E.J. Ya, Y. Xin, Applied Surface Science 255 (2009) 6415–6420.
[40] M.G. Walter, E.L. Warren, J.R. Mckone, S.W. Boettcher, Q.X. Mi, E.A. Santori, N.S. Lewis, Chemical Reviews 110 (2010) 6446–6473.
[41] Z.H. Zhang, L.B. Zhang, M.N. Hedhili, H.N. Zhang, P. Wang, Nano Letters 13 (2013) 14–20.
[42] C.Z. Li, Frontiers of Chemical Engineering in China 4 (2010) 18–25.
[43] S. Rengaraj, S.H. Jee, S. Venkataraj, Y. Kim, S. Vijayalakshmi, E. Repo, A. Koistinen, M. Sillanpää, Journal of Nanoscience and Nanotechnology 11 (2011) 1–10.
[44] S.L. Liu, Z.Q. Wang, H. Liu, Q.Q. Xu, Journal of Materials Research 28 (2013) 2970–2976.
[45] D.D. Wagman, W.H. Evans, V.B. Parker, R.H. Schumm, I. Halow, S.M. Bailey, K.L. Churney, R.L. Nuttall, Journal of Physical and Chemical Reference Data 18 (1989) 1807.